Constitutively active Notch4 receptor elicits brain arteriovenous malformations through enlargement of capillary-like vessels

Patrick A. Murphy[a,1,2], Tyson N. Kim[a,1], Lawrence Huang[a,1], Corinne M. Nielsen[a], Michael T. Lawton[b], Ralf H. Adams[c], Chris B. Schaffer[d], and Rong A. Wang[a,3]

[a]Laboratory for Accelerated Vascular Research, Department of Surgery, Division of Vascular Surgery, University of California, San Francisco, CA 94143; [b]Department of Neurosurgery, University of California, San Francisco, CA 94143; [c]Max Planck Institute for Molecular Biomedicine, Faculty of Medicine, Department of Tissue Morphogenesis, University of Münster, D-48149 Münster, Germany; and [d]Department of Biomedical Engineering, Cornell University, Ithaca, NY 14853

Edited by Michael A. Gimbrone, Brigham and Women's Hospital, Boston, MA, and approved November 11, 2014 (received for review August 13, 2014)

Arteriovenous (AV) malformation (AVM) is a devastating condition characterized by focal lesions of enlarged, tangled vessels that shunt blood from arteries directly to veins. AVMs can form anywhere in the body and can cause debilitating ischemia and life-threatening hemorrhagic stroke. The mechanisms that underlie AVM formation remain poorly understood. Here, we examined the cellular and hemodynamic changes at the earliest stages of brain AVM formation by time-lapse two-photon imaging through cranial windows of mice expressing constitutively active Notch4 (Notch4*). AVMs arose from enlargement of preexisting microvessels with capillary diameter and blood flow and no smooth muscle cell coverage. AV shunting began promptly after Notch4* expression in endothelial cells (ECs), accompanied by increased individual EC areas, rather than increased EC number or proliferation. Alterations in Notch signaling in ECs of all vessels, but not arteries alone, affected AVM formation, suggesting that Notch functions in the microvasculature and/or veins to induce AVM. Increased Notch signaling interfered with the normal biological control of hemodynamics, permitting a positive feedback loop of increasing blood flow and vessel diameter and driving focal AVM growth from AV connections with higher blood velocity at the expense of adjacent AV connections with lower velocity. Endothelial expression of constitutively active Notch1 also led to brain AVMs in mice. Our data shed light on cellular and hemodynamic mechanisms underlying AVM pathogenesis elicited by increased Notch signaling in the endothelium.

vascular anomaly | angiogenesis | stroke | hereditary hemorrhagic telangiectasia | Notch

Proper vascular perfusion requires a capillary interface between arteries and veins. Establishing and preserving the arteriovenous (AV) interface are critical for tissue function. AV malformation (AVM) is a pathological perturbation of the AV interface and is characterized by enlarged, tangled vessels that shunt blood directly from arteries to veins lacking intervening capillaries (1). Brain AVMs can cause ischemia, intracerebral hemorrhage, disability, stroke, and death. About half are first diagnosed between 20 and 40 y of age (1), accounting for 50% of childhood stroke (2). The developmental mechanisms of AVM pathogenesis remain poorly understood, hindering the development of therapeutic treatment strategies.

Clinical evidence has led to two theories about the origin of brain AVM. First, brain AVMs are congenital and caused by failed regression of embryonic AV connections that persist into postnatal life (3). This theory is based on morphological interpretation of AVMs that resemble primitive vascular structures. However, the lack of detection by prenatal ultrasonography suggests that AVMs are either too small to detect in fetal stages or they develop after birth. The second theory suggests that AVMs result from improper remodeling of venules (4). Examination of biopsies from skin telangiectases in humans suggests that enlargement of postcapillary venules precedes AVM formation and can occur in postnatal life (5). However, the critical precipitating event remains unknown.

Loss-of-function mutations identified in the familial disease Hereditary Hemorrhagic Telangectasia (HHT), including the TGF-β family receptor Alk1 (HHT2) (6) and its coreceptor endoglin (HHT1) (7), have provided valuable models to study the molecular basis of AVMs. Genetic deletion of each of these genes has revealed that they are required for normal vascular development and prevention of AVM formation (6–8). Mutations in *SMAD4*, *RASA1*, and *PTEN* have also been linked to AVMs in humans (9, 10), and mutations in *Rasa1* lead to AV shunting in zebrafish (11).

The Notch receptors are transmembrane proteins that promote arterial endothelial cell (EC) specification by enhancing expression of arterial molecular markers and suppressing the expression of venous markers (12–19). Abnormal signaling induces enlarged AV connections and shunting in mouse and zebrafish embryos (12–14). Notch activity is aberrantly increased in the endothelium of human brain AVMs (18, 20), suggesting that it may participate in the growth or maintenance of human AVMs. These findings offer exciting opportunities to understand the molecular mechanisms of AVM formation. We have previously reported a mouse model, *Tie2-tTA;TRE-Notch4** or Tie2-Notch4* mice, wherein postnatal expression of constitutively active Notch4 (Notch4*) in

Significance

Brain arteriovenous malformations are focal lesions of enlarged, tangled vessels that shunt blood from arteries directly to veins. They can cause ischemia, hemorrhage, disability, and death, particularly in young people, accounting for 50% of childhood stroke. The molecular etiology of the disease remains poorly understood, hindering the development of therapeutic treatments. Here, we report that, in an animal model, the lesion arises from the enlargement of capillary-like vessels. Notch signaling in the endothelium of microvasculature and veins is critical for the disease initiation by increasing cell areas but not proliferation. Blood flow mediates disease progression by a positive feedback of increasing flow and vessel diameter. Our data shed light on the mechanism underlying the pathogenesis of this devastating disease.

Author contributions: P.A.M., T.N.K., L.H., C.M.N., C.B.S., and R.A.W. designed research; P.A.M., T.N.K., L.H., and C.M.N. performed research; R.A.W. supervised the project; T.N.K., R.H.A., and C.B.S. contributed new reagents/analytic tools; P.A.M., T.N.K., L.H., C.M.N., M.T.L., C.B.S., and R.A.W. analyzed data; M.T.L. provided medical relevance; and P.A.M., T.N.K., L.H., and R.A.W. wrote the paper.

The authors declare no conflict of interest.

This article is a PNAS Direct Submission.

[1]P.A.M., T.N.K., and L.H. contributed equally to this work.

[2]Present address: Koch Institute for Integrative Cancer Research, Massachusetts Institute of Technology, Cambridge, MA 02139.

[3]To whom correspondence should be addressed. Email: rong.wang@ucsfmedctr.org.

This article contains supporting information online at www.pnas.org/lookup/suppl/doi:10.1073/pnas.1415316111/-/DCSupplemental.

ECs results in spontaneous AVMs in mice (15–17, 21). Although this work has facilitated new research directions regarding the Notch pathway in AVMs, how aberrant Notch signaling leads to AVM remains unknown. Elucidating the initiating structural events that lead to AV shunt formation would provide insight into AVM pathogenesis.

A major obstacle to understanding AVM pathogenesis has been the inability to observe AVM formation and blood flow over time with high-resolution in vivo imaging. Here, we examined AVM formation in Tie2-Notch4* mice from the initial genetic event, illuminating disease progression using "5D" two-photon imaging, which allows high-resolution live imaging of vascular architecture (3D) and blood velocity (the fourth dimension) over time (the fifth dimension) (16, 22, 23). Our findings provide insights into the mechanism of brain AVM formation.

Results

Notch4*-Mediated AV Shunts Arise from the Enlargement of Capillary-Like Vessels. To determine the developmental origin of AVMs, we performed longitudinal live imaging in the brains of Tie2-Notch4* mice, in which Notch4* expression was repressed until birth by tetracycline treatment. We implanted cranial windows over the right parietal cortex of mice at postnatal day 7 (P7) and used in vivo two-photon microscopy to record vessel diameter and blood velocity over time. We measured lumen diameters of vessels connecting arteries and veins, or AV connections, at their narrowest point. We defined measurements ≥12.5 μm as AV shunts because AV connections of this diameter were not observed in control mice after P12 (*SI Appendix*, Fig. S1). We found that AV shunts developed from capillary-like vessels in Tie2-Notch4* mice beginning at ~P12 (Fig. 1 and *SI Appendix*, Figs. S2 and S3). Of 109 of the AV connections that we tracked, 41 (38%) grew to ≥12.5 μm between P14 and P25 in 12 mutants, and 4 of 109 (4%) grew to ≥30 μm (Fig. 1*A* and Movies S1 and S2). However, the initial diameter did not differ from that of controls (5.4 ± 1.6 vs. 5.3 ± 1.6 μm, Fig. 1*B*). We saw no correlation between the final and initial diameters of AV shunts (*SI Appendix*, Fig. S4). We conclude that AV shunts in Tie2-Notch4* mice enlarge from capillary-diameter AV connections, but that only a few continue to grow into large AVMs.

We examined the hemodynamics of AV shunts at their onset and as they enlarged. Using 5D two-photon imaging (16, 23), we simultaneously analyzed red blood cell velocity and AV connection diameter (Fig. 1 *C–E* and *SI Appendix*, Fig. S2). AV

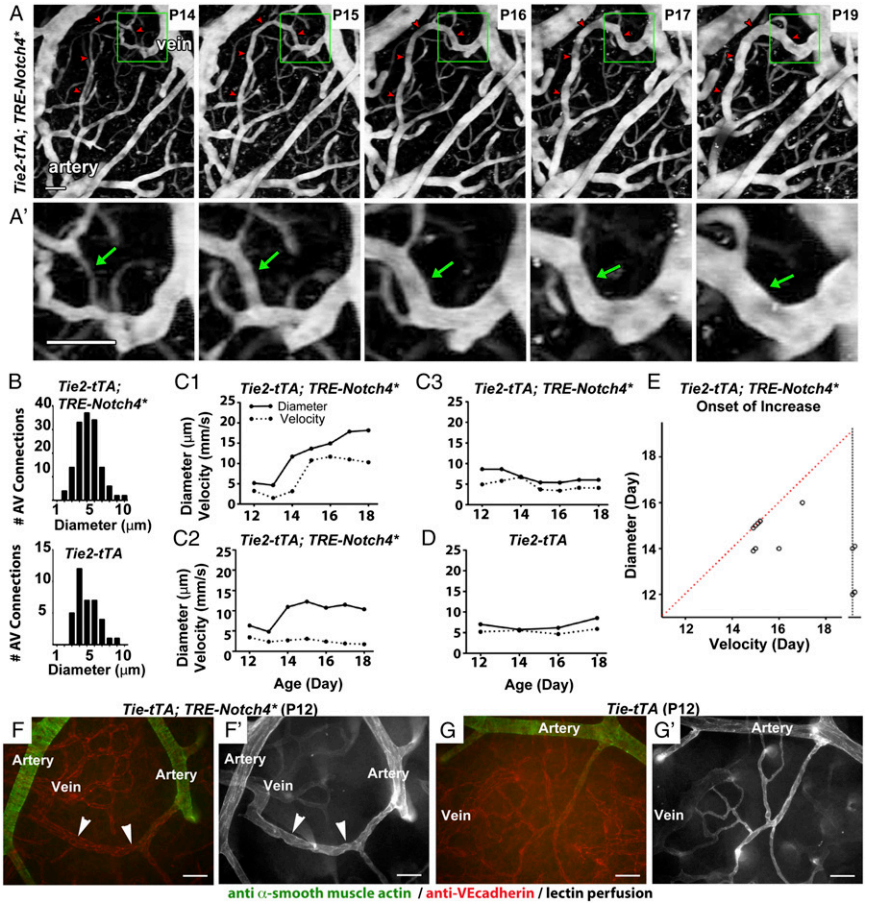

Fig. 1. *Tie2-tTA;TRE-Notch4** mice developed AV shunts through enlargement of capillary-like vessels. (*A* and *A'*) Two-photon time-lapse imaging of FITC-dextran–labeled AV connections in the cerebral cortex through a cranial window. An AV shunt (red arrowheads and green arrows) developing from a capillary-diameter AV connection between P14 and P19. (*B*) Distribution of initial AV connection diameter (smallest lumen diameter) in AV connections in mutants (109 AV connections in 12 mice) and controls (36 AV connections in 5 mice, ages P8–P11). (*C* and *D*) Blood velocities (dotted lines) and lumen diameters (solid lines) measured over time in the capillary-like AV connections of (*C1–C3*) *Notch4** mice and (*D*) controls. (*E*) Time of initial velocity increase vs. time of initial diameter increase for individual AV connections. Dotted red line represents simultaneous increase of blood velocity and vessel diameter. Points on the dotted vertical black line represent capillary-like vessels that enlarged but did not exhibit a significant increase in velocity. Increased velocity and diameter were defined by changes >2× the SD in control capillaries: 0.82 mm/s for velocity and 1.33 μm for diameter. (*F* and *G*) Whole-mount immunostaining of P12 surface cerebral cortex vasculature for α-smooth muscle actin (green) and VE-cadherin (red) in mutant (*F*) and control (*G*). Arrowheads indicate AV shunt (18 AV shunts in seven mice); corresponding lectin perfused vessels are shown (*F'* and *G'*). (Scale bars, 50 μm.)

connection enlargement either coincided with or preceded the initial increase in velocity (Fig. 1*C1*, 8/18 vessels in four mice). Some capillary-like vessels enlarged without a significant increase in velocity (Fig. 1*C2*, 4/18 vessels in four mice), whereas others exhibited an increase in neither diameter nor velocity (Fig. 1*C3*, 6/18 vessels in four mice). Neither velocity nor diameter increased in controls (Fig. 1*D*, 18 vessels in four mice). Data are summarized in Fig. 1*E*. Thus, our data suggest that blood velocity in AV connections that grew into AV shunts is initially capillary-like and becomes abnormally elevated only when connections enlarge.

As capillaries lack smooth muscle cell (SMC) coverage, we performed staining for α-smooth muscle actin (SMA) at P12, when AV shunts were first apparent. We identified 10 AV shunts from five mice that lacked SMA staining (Fig. 1*F*). In contrast, adjacent arteries were positive for SMA staining, similar to controls (Fig. 1*G* and *SI Appendix*, Fig. S5). We observed, as we have previously published (15–17), that advanced AVMs exhibited increased SMA staining. Thus, the absence of SMCs in the initial AV shunts is consistent with a capillary origin of AVMs in the Tie2-Notch4* mice.

We next examined the expression of Notch4* during the initiation of AV shunting. We previously demonstrated that Tie2-tTA effectively and specifically drives gene expression throughout the brain endothelium, through activation of the tetracycline responsive element (TRE) by the tetracycline transactivator (tTA) (17). Here we performed whole-mount staining of brain vasculature for the Notch4 intracellular domain (ICD), which also detects Notch4*, without the extracellular domain. We detected elevated Notch4-ICD throughout vasculature (reflecting Notch4* expression) in the mutants over the controls (*SI Appendix*, Fig. S6).

To examine the kinetics of Notch4* expression in real time during AV shunt formation, we analyzed *TRE-H2b-eGFP*; *Tie2-tTA; TRE-Notch4** mice. *TRE-H2b-eGFP* reports tTA activity and thus *TRE-Notch4** expression. As expected, there was a positive correlation between H2b-eGFP intensity and Notch4* expression in fixed samples, validating the reporter assay (*SI Appendix*, Fig. S7). We found that tTA activity preceded, by about 2 d, the enlargement in each segment (branch point to branch point) of the AV connections measured (Fig. 2 *A*–*C*). Approximately 80% (159/198) of segments were positive for the *TRE-H2b-eGFP* reporter (Fig. 2*D* and *SI Appendix*, Fig. S8). About 50% (83/159) of the positive segments enlarged, and 40% (59/159) of these became part of AV shunts ≥12.5 μm in diameter. Only 15% (24/159) regressed (Fig. 2*D* and *SI Appendix*, Fig. S8). In contrast, only 10% of the H2b-eGFP–negative segments enlarged (4/39); 80% (31/39) regressed. These data suggest that Notch4* expression promptly leads to AV shunting.

EC Area, but Not Number or Proliferation, Increased in AV Shunt Formation. To examine the cellular changes underlying the initiation of AV shunts, we used the *R26R-confetti* reporter (24) to track the position and number of labeled cells. We activated the reporter from P1 to P5 by tamoxifen (TAM) induction of *Cdh5 (PAC)-CreERT2* in *Tie2-tTA;TRE-Notch4*; Cdh5(PAC)-CreERT2; R26R-Confetti* mice and littermate controls (with either *TRE-Notch4** or *Tie2-tTA*, but not both), allowing the tracking of ECs during AV shunt formation (Fig. 3*A*). Surprisingly, we saw no detectable increase in cell number in the initial 48 h of AV shunt formation (Fig. 3 *A* and *B* and *SI Appendix*, Fig. S9), despite a two- to threefold increase in AV shunt diameter (Fig. 3*B*). Because our analysis was powered to detect as little as a twofold difference in cell number, these data suggest that AV shunt growth does not occur through a simple increase in EC number.

To investigate whether cell proliferation is involved in the initiation of AV shunts, we performed BrdU analysis of tomato-lectin–labeled ECs. This assay showed no significant difference in the number of BrdU+ ECs (labeled for 48 h leading up to the analysis, Fig. 3 *C* and *D* and *SI Appendix*, Fig. S10). Furthermore, we found no BrdU+ EC cells in 10/15 AV shunts with diameters ≥12.5 μm, again suggesting that the initiation of the AV shunt does not require increased EC proliferation.

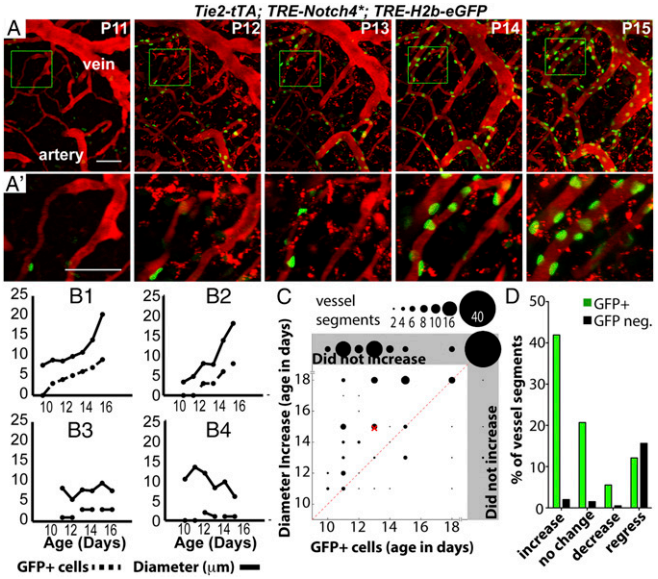

Fig. 2. Notch4 expression increased in brain capillaries before enlargement of AV shunts. (*A* and *A′*) Two-photon imaging of an AV connection from P11 to P16; Texas-Red–dextran labels plasma (red) and TRE-H2b-eGFP indicates tTA activity (green). (*B1–B4*) Diameter vs. number of GFP+ cells in vessel segments: increased (*B1* and *B2*), stable (*B3*), and decreased (*B4*) diameter. (*C*) Correlation between time of initial detection of GFP+ cells and initial diameter increase in capillary-diameter vessel segments of Notch4* mice. Gray regions indicate that GFP+ cells were not detected or diameter increase was not detected or both. Dotted line represents simultaneous detection of GFP+ cells and diameter increase. The "×" indicates the means. GFP was detected before (125/198 vessel segments, five mice), or simultaneous with enlargement (19/198) in most cases. (*D*) Percentage of vessel segments (TRE-eGFP+ or negative) that demonstrated an increase, decrease, or no change in diameter or that completely regressed. Increased or decreased diameter is defined by >2× the SD of change in control vessels (1.1 μm) in the same period; segments are defined by branch points. (Scale bars: *A*, 100 μm; *C*, 50 μm.)

We hypothesized that a change in the area covered by individual ECs might support the capillary enlargement in Tie2-Notch4* mice. To test this, we stained whole-mount cortical sections of mutants and controls for vascular endothelial cadherin (VE-cadherin, Cdh5) during the initial stages of AV shunt formation (P12). We found that the area covered by individual ECs increased more than threefold during the early stages of AV shunt formation (Fig. 3 *E* and *F*, mean cell area of 157 ± 24 μm^2 in three *Tie2-tTA* mice and 540 ± 46 μm^2 in five *Tie2-tTA;TRE-Notch4** mice with AV shunts ≥12.5 μm; $P = 0.0001$ by two-tailed Student *t* test). Thus, an increase in EC area correlates with the enlargement of capillaries in AV shunt formation.

Notch4* Expression in ECs of Arteries Was Not Sufficient to Induce AV Shunt Formation. We asked where in the vascular tree Notch4* acts to elicit AV shunt formation. Our in vivo imaging suggested that a defect in the capillaries or microcirculation led to AV shunts. Because no capillary EC-specific tTA driver has been reported, we used *Cdh5(PAC)-CreERT2* to induce Notch4* in all ECs and a recently developed arterial-specific line, *BMX(PAC)-CreERT2*, to examine the effects of Notch4* specifically in the arterial ECs.

We first confirmed the expression of the two inducible Cre lines in our system. *Cdh5(PAC)-CreERT2* efficiently activated a mT/mG Cre-reporter throughout the vascular endothelium, but not in circulating blood cells (*SI Appendix*, Figs. S11 and S12). The *ROSA:LNL:tTA* system effectively induced *Notch4** expression, resulting in even higher protein levels than *Tie2-tTA*–driven expression (*SI Appendix*, Fig. S13 and Movie S3) (25). As demonstrated in other tissues (26), *BMX(PAC)-CreERT2* efficiently activated the same reporter throughout the arterial trunk

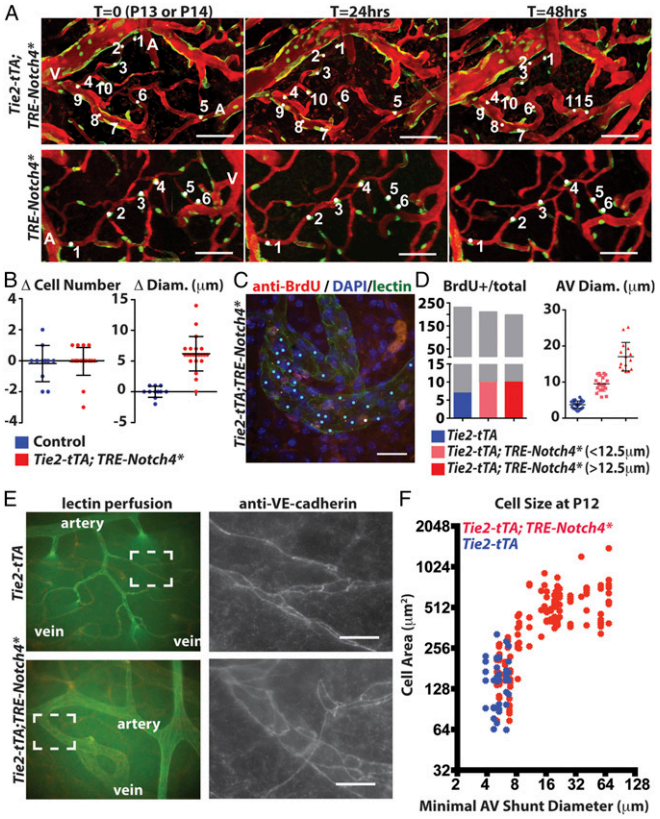

Fig. 3. Endothelial growth in the AV shunt accompanied by the expansion of endothelial cell surface area. (*A*) Two-photon time-lapse imaging showing *Cdh5 (PAC)-CreER; Confetti*-marked nuclear GFP+ and cytoplasmic YFP+ ECs in cerebral cortex of mutants and controls. Texas-Red–dextran labels plasma. (*B*) Quantification of total cell number and AV connection diameter over the same interval (22 AV connections in five mutants, 11 AV connections in three controls). (*C*) Whole-mount BrdU staining/lectin perfusion. P12 AV connection from mutant cerebral cortex is shown. Blue dots indicate Hoechst+/lectin+ cells. White dots indicate BrdU+/lectin+ cells. (*D*) Quantification of BrdU+ ECs, total ECs, and AV connection diameter (34 connections in controls, 20 AV connections <12.5 μm in five mutants, and 15 AV connections ≥12.5 μm in four mutants). Gray indicates all Hoechst+/lectin+ cells, and the colored portion indicates the number of BrdU+/lectin+ cells. (*E*) Whole-mount staining of P12 cerebral cortex for VE-cadherin, counterstained by lectin perfusion. (*F*) Correlation of size of VE-cadherin–traced cells in P12 control (blue) and Notch4* (red) connections with AV connection diameter (24 AV connections in 11 mutants, 6 AV connections in three controls). (Scale bars: *A*, 100 μm; *C* and *E*, 25 μm.)

in the brain vasculature (*SI Appendix*, Fig. S11). Examination of mice with combined expression of the arterial marker *ephrin-B2-H2b-eGFP* and *BMX(PAC)-CreERT2;mT/mG* revealed that *BMX (PAC)-CreERT2* excision overlapped with *ephrin-B2-H2b-eGFP* in arteries but not in microvessels (*SI Appendix*, Fig. S14 and Movie S3). Therefore, *BMX(PAC)-CreERT2* was uniformly active in arteries but not small arterioles. As such, the *Cdh5(PAC)-CreERT2; ROSA:LNL:tTA* driver induces Notch4* expression throughout the vascular endothelium, similar to the Tie2-tTA system, whereas the *BMX(PAC)-CreERT2; ROSA:LNL:tTA* driver induces Notch4* specifically in the endothelium of arteries.

To evaluate the formation of AV shunts, we examined tomato-lectin–perfused whole-mount preparations of *Cdh5(PAC)-CreERT2; ROSA:LNL:tTA;TRE-Notch4** and *BMX-CreERT2; ROSA:LNL:tTA;TRE-Notch4** at P18, when most Tie2-Notch4* mice have developed AV shunts (17). As expected, we readily detected enlarged AV connections in *Cdh5(PAC)-CreERT2; ROSA: LNL:tTA ;TRE-Notch4** mice by P18 after TAM injection at P7–P8 to induce Cre-mediated tTA expression (Fig. 4*A* and *SI Appendix*, Table S1). In these mice, 82.8 ± 21.8% of total AV connections were enlarged. By contrast, the *BMX-CreERT2;ROSA: LNL:tTA;TRE-Notch4** mice resembled the negative littermate controls with only 2.1 ± 3.6% of total AV connections enlarged (Fig. 4 *B* and *C* and *SI Appendix*, Table S1). Therefore, expression of Notch4* in the endothelium of *BMX-CreERT2* positive arteries is not sufficient to induce AV shunts in the brain.

Rbpj in the ECs of *BMX-CreERT2*–Negative, but Not *BMX-CreERT2*–Positive Arteries, Was Required for Notch4*-Induced AV Shunt Formation. To investigate the molecular mediator of Notch4*-induced AV shunt formation, we examined Rbpj, a transcription factor required for canonical Notch signaling. We deleted *Rbpj* in *Tie2-tTA;TRE-Notch4*;Cdh5(PAC)-CreERT2;Rbpj$^{f/f}$* mice before the onset of AV shunts by injecting TAM at P7–P8. Excision of *Rbpj* using *Cdh5(PAC)-CreERT2* effectively suppressed AV shunt formation, and only 1.2 ± 1.7% of total AV connections were enlarged by P18 (Fig. 4*D* and *SI Appendix*, Table S2). In contrast, in controls with one remaining *Rbpj* allele, 22.3 ± 17.2% of total AV connections were enlarged (Fig. 4*E* and *SI Appendix*, Table S2). Thus, Notch4*-induced AV shunts require canonical Notch signaling via Rbpj.

Because AV shunts were Rbpj-dependent, we tested whether blocking arterial Notch signaling suppresses AV shunt formation. We deleted *Rbpj* by injecting TAM at P7–P8 in arterial ECs of *Tie2-tTA;TRE-Notch4*; BMX(PAC)-CreERT2;Rbpj$^{f/f}$* mice. Excision of both *Rbpj* alleles using *BMX(PAC)-CreERT2* did not suppress the AV shunt phenotype, because we found that 62.7 ± 27.5% of total AV connections were enlarged by P18 (Fig. 4*F* and *SI Appendix*, Table S2), which is no different from mice with excision of only one *Rbpj* allele [60.1 ± 36.4% of total AV connections enlarged (*SI Appendix*, Table S2)]. Taken together, these data suggest that the onset of AV shunts is mediated through Rbpj in the ECs of microvasculature and veins but not *BMX(PAC)-CreERT2*–positive arteries.

AV Shunts with Higher Velocity Increased in Velocity and Diameter, Whereas Adjacent Vessels with Lower Velocity Decreased in Velocity and Diameter. Despite Notch4* expression throughout the vascular endothelium, not all AV connections developed into AV shunts, and not all AV shunts continued to enlarge. We

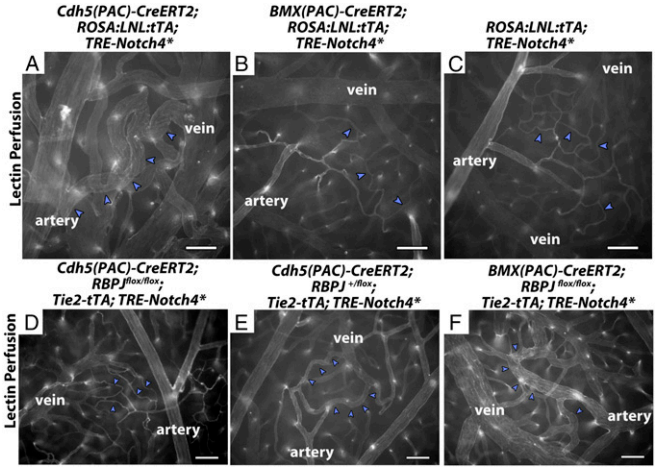

Fig. 4. Changes in Notch signaling in the artery alone did not affect AV shunt formation. (*A–F*) Lectin-perfused vasculature on P18 surface cerebral cortex. (*A* and *B*) *ROSA:LNL:tTA;Notch4** mice in which Notch4* was expressed at P7 with temporally inducible Cre-recombinase. (*D–F*) *Notch4** mutant or control mice with Cre-mediated *RBPJ* deletion at P7. (*A*) $n = 83$ AV connections in three mice. (*B*) $n = 43$ AV connections in three mice. (*C*) $n = 103$ AV connections in three mice. (*D*) $n = 191$ AV connections in five mice. (*E*) $n = 186$ AV connections in six mice. (*F*) $n = 171$ AV connections in seven mice. Blue arrowheads indicate AV connections. (Scale bars, 100 μm.)

investigated whether differences in blood flow velocity determine the growth of AV shunts. We identified arterial branch points in mutant mice in which one branch clearly led into an AV shunt (V1 in Fig. 5 *A* and *B*). We measured velocity and diameter in the higher-velocity AV shunt and the lower-velocity adjacent artery (V2 in Fig. 5 *A* and *B*) over time in Tie2-Notch4* mice and compared the changes in velocity and diameter to control arteries (V1 and V2 in Fig. 5 *C* and *D*). The velocities in control arteries were more stable, varying by an average of 16% between time points vs. 45% in the mutants. In five of seven cases where the velocity in the AV shunt increased, the velocity in the adjacent artery with lower velocity decreased [compare Fig. 5 *A* to *B*; see summary in Fig. 5*E* "when AV shunt velocity increases" (see example in Movie S4)]. In three cases, the velocity was reduced in both the AV shunt and its adjacent artery (Fig. 5*E*, "when AV shunt velocity decreases"). The velocity in control arteries did not change (Fig. 5*E*, "control"). Thus, increased velocity in AV shunts is often accompanied by decreased velocity in the adjacent arteries of Tie2-Notch4* mice.

We then investigated whether changes in velocity correlated with changes in diameter in Tie2-Notch4* mutants. We focused on the AV shunts in which velocity increased and adjacent arteries in which velocity decreased (represented by red dots in Fig. 5*E*). We found that the adjacent downstream arteries indeed regressed, compared with either the AV shunt or arteries measured in control mice (Fig. 5*F*, $P < 0.02$ by two-tailed Student *t* test, V2 in Fig. 5 *A* and *B*, and *SI Appendix*, Fig. S15). Therefore, changes in velocity correlated with changes in diameter, so that the highest velocity connections, which also tended to be the most proximal AV connections in the Tie2-Notch4* mice, exhibited increasing velocity and diameter, whereas the lower velocity and typically distal arterial branches exhibited reduced velocity and diameter.

For a broader perspective on AV shunt progression, we examined the whole brain by casting the vessels with radio-opaque microfil and imaging with microCT. Despite widespread AV shunting in mutant mice, AVM development appeared focal (Fig. 5*G*). Thus, our data suggest that the unchecked growth of higher-velocity AV connections results in focal AVM development.

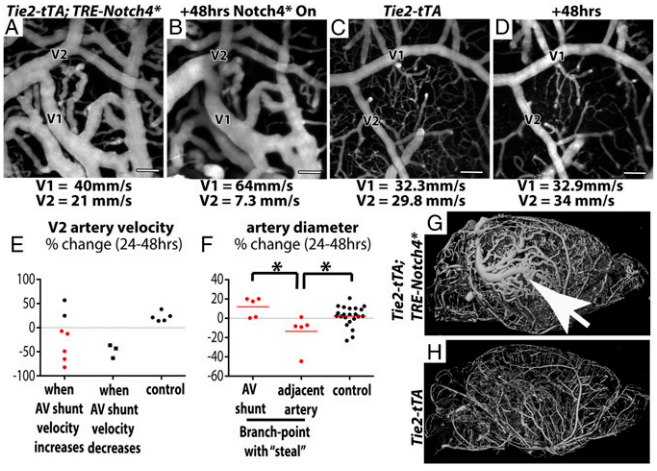

Fig. 5. AV shunts with higher velocity enlarged whereas adjacent arteries with lower velocity reduced in caliber. (*A–D*) Two-photon time-lapse imaging of FITC-dextran–labeled blood vessels on cerebral cortex through a cranial window. Average blood velocity, as determined by line-scan analysis of single RBCs is indicated for the AV shunt (V1) and the adjacent artery (V2) in a mutant (*A* and *B*) and control (*C* and *D*). (*E*) Change in velocity over 24–48 h in distal arteries from Notch4* AV shunts when shunt velocity increased ($n = 7$) or decreased ($n = 3$), and in the smaller artery of similar branch points in controls ($n = 5$). (*F*) Change in diameter of AV shunts and adjacent arteries in the subgroup of *Notch4** mice in which AV shunt velocity increased and distal velocity decreased (red points in *E*). (*G* and *H*) MicroCT of microfil-labeled whole-brain vasculature in (*G*) *Notch4** and (*H*) control mice. Arrow indicates focal aggregation of enlarged arteries and veins. *$P < 0.05$. (Scale bars, 100 μm.)

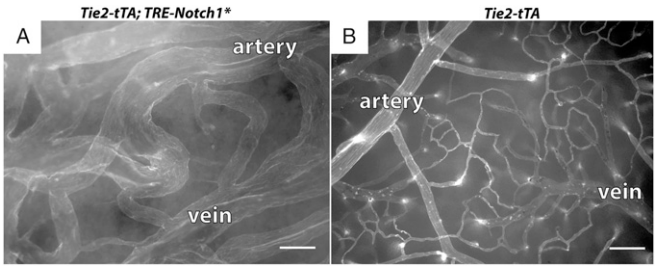

Fig. 6. Endothelial expression of Notch1-ICD induced AV shunts. Lectin-perfused vasculature of P14 (*A*) Tie2-tTA; TRE-Notch1* mutant and (*B*) littermate control. (Scale bar, 100 μm.)

Endothelial Expression of Activated Notch1 Induced AV Shunt Formation. To determine whether expression of constitutively active Notch1 in the endothelium also causes AV shunt formation, we combined a constitutively active, tTA-responsive *Notch1** allele (16) with *Tie2-tTA* and activated Notch1* at birth. Five of five *Tie2-tTA;TRE-Notch1** mice exhibited signs of ataxia or lethargy by P14, as well as large brain AVMs, whereas none of six controls were affected (Fig. 6). Thus, endothelial expression of constitutively active Notch1 induces brain AV shunts during neonatal development.

Discussion

Here, we provide novel mechanistic insights into AVM formation. Our data suggest that AV shunts arise from the enlargement of capillary-like vessels and that cell-autonomous Notch signaling in the endothelium of microvasculature and veins is sufficient and required for AVM formation. AV shunt initiation is accompanied by the enlargement of EC area but not increased proliferation. Blood flow mediates AV shunt progression by positive feedback of increasing flow and increasing diameter, leading to the selective growth of focal AVMs.

Our data shed light on the origin of AVMs. The vascular structure of brain AVMs has led to speculations that they arise from failed regression of primitive AV connections during development (3, 4). Extrapolation of histological analysis of skin AVMs led others to propose that brain AVMs arise from the dilation of postcapillary venules (5). In contrast to the existing models, our results demonstrate that Notch4*-induced AV shunts grow from preexisting capillary-like connections with no detectable differences from normal capillaries in either their diameter or their velocity. This suggests a new, potentially capillary-originated model of AVM initiation.

Endothelial but not hematopoietic Notch signaling is critical in the formation of AV shunts. Previous work has demonstrated a critical function for blood cells in separating the blood and lymphatic vascular systems (27). Our data, confirmed by two independent induction systems, demonstrate that increased Notch signaling specifically within the endothelium is sufficient to cause AV shunt formation without obvious involvement of the blood cells. Conversely, expression of Notch4* specifically in *Scl-tTA*–positive blood lineages did not lead to AV shunt formation (*SI Appendix*, Fig. S16). Furthermore, no increase in CD45+ cells was observed near AV shunts (*SI Appendix*, Fig. S17). Together, our data suggest that expression of Notch4* in the blood lineages is insufficient to induce AV shunts and that endothelial Notch4* elicits AVMs in a cell-autonomous fashion.

Initial enlargement of AV shunts correlates with area expansion of individual ECs, rather than increased proliferation. Consistent with this finding, we found that the converse is true: EC area is reduced during AV shunt regression upon turning off the

*Notch4** transgene (16). Further investigation is required to determine whether an altered cell area is a direct or indirect effect of Notch4*. Whether further enlargement of AV shunts beyond the initial stage depends on cell proliferation is currently unknown. We speculate that the growth of the AV shunts eventually requires cell proliferation because AV shunts in symptomatic mice can be >10-fold larger than normal capillaries.

Notch signaling in the microvasculature and veins is both sufficient and required for AVM formation. Arterial *BMX(PAC)-CreERT2*–mediated up- or down-regulation of Notch signaling could not induce or suppress AV shunt formation, respectively. In the same genetic systems, global endothelial *Cdh5(PAC)-CreERT2*–mediated up- or down-regulation could. These findings are consistent with recent work showing that Rbpj-mediated arterial Notch signaling is dispensable for postnatal artery formation in the retina (26). Together, these data show that changes in Notch signaling in the *BMX(PAC)-CreERT2* active cells are not critical in AV shunt formation, implying that it induces AVM through effects on the microvasculature and veins.

Blood flow is a key regulator of vessel caliber (28). Based on clinical studies, it has been proposed that increased flow through low-resistance AV shunts encourages their growth while "stealing" blood flow from adjacent higher-resistance vessels (29). However, previous studies have typically focused on a single time point with lower resolution than we show here. We provide experimental evidence that endothelial Notch4* permits a "steal" and perpetuates a positive feedback loop, leading to selective growth of higher-velocity connections at the expense of lower-velocity connections.

Our data also demonstrate that, in controls, blood velocity in adjacent two-branch arteries is maintained at a comparable rate over time. In mutants, the blood velocity in adjacent two-branch arteries varies greatly and with increasing disparity. Our earlier work shows that turning off Notch4* expression normalizes high-velocity AV shunts by rapidly reducing the flow and diameter of the AV shunt while increasing flow and diameter to the distal artery (16). Together, these findings suggest that sustained endothelial expression of Notch4* compromises biological checks that prevent AV connections from enlarging and "stealing" flow from adjacent vessels.

We believe that normal AV specification is critical in maintaining proper hemodynamics in the vasculature. Because Notch signaling is a critical determinant of AV specification, it is conceivable that either gain or loss of Notch activity could disrupt AV specification, compromising normal vascular control of hemodynamic forces and leading to AVMs. Indeed, both gain- and loss-of-function Notch mutants develop abnormal shunting in mouse embryos (13, 30). Our model is consistent with recent work hinting that reduced Notch signaling in HHT type 2 could contribute to AVMs (31). We propose that increased Notch signaling in the endothelium of nonarterial vessels disturbs biological control of blood flow by allowing the persistent growth of high-flow AV connections at the expense of lower flow AV connections (*SI Appendix*, Fig. S18).

Materials and Methods

See *SI Appendix* for detailed information on materials and methods. Cranial windows, in vivo imaging, lectin-perfusion, Notch4-ICD, SMA, and VE-cadherin immunostaining was as we described (16). BrdU immunostaining was as described (32). For peripheral blood isolation, blood was removed from right ventricles, and erythrocytes were lysed. Flow cytometry was performed following CD45 immunostaining and DAPI labeling. For MicroCT, images of Microfil-labeled vasculature were acquired using a μCT 40 system (Scanco Medical AG). All mouse lines used have been published. This study was carried out in strict accordance with National Institute of Health regulations and the Institutional Animal Care and Use Committee at the University of California, San Francisco.

ACKNOWLEDGMENTS. This work was supported by National Institutes of Health (NIH) Grants R01 NS067420 and R56NS06742, Vascular Cures (formerly the Pacific Vascular Research Foundation), the Frank A. Campini Foundation, the Mildred V. Strouss Trust, American Heart Association (AHA) Grant-in-Aid 10GRNT4170146 and GRNT 16850032, NIH Grant R01 HL075033 (to R.A.W.), AHA Grant 0715062Y and Tobacco-Related Disease Research Program (TRDRP) 18DT-0009 Predoctoral Fellowships (to P.A.M.), TRDRP 19DT-007 and NIH F30 1F30HL099005-01A1 Predoctoral Fellowships (to T.N.K.), and TRDRP 20FT-0069 and NIH F32 1F32HL110724-01A1 Postdoctoral Fellowships (to C.M.N.).

1. Friedlander RM (2007) Clinical practice. Arteriovenous malformations of the brain. *N Engl J Med* 356(26):2704–2712.
2. Meyer-Heim AD, Boltshauser E (2003) Spontaneous intracranial haemorrhage in children: Aetiology, presentation and outcome. *Brain Dev* 25(6):416–421.
3. Mullan S, Mojtahedi S, Johnson DL, Macdonald RL (1996) Embryological basis of some aspects of cerebral vascular fistulas and malformations. *J Neurosurg* 85(1):1–8.
4. Lasjaunias P (1997) A revised concept of the congenital nature of cerebral arteriovenous malformations. *Interventional Neuroradiol* 3(4):275–281.
5. Braverman IM, Keh A, Jacobson BS (1990) Ultrastructure and three-dimensional organization of the telangiectases of hereditary hemorrhagic telangiectasia. *J Invest Dermatol* 95(4):422–427.
6. Park SO, et al. (2009) Real-time imaging of de novo arteriovenous malformation in a mouse model of hereditary hemorrhagic telangiectasia. *J Clin Invest* 119(11): 3487–3496.
7. Mahmoud M, et al. (2010) Pathogenesis of arteriovenous malformations in the absence of endoglin. *Circ Res* 106(8):1425–1433.
8. Chen W, et al. (2014) De novo cerebrovascular malformation in the adult mouse after endothelial Alk1 deletion and angiogenic stimulation. *Stroke* 45(3):900–902.
9. Uebelhoer M, Boon LM, Vikkula M (2012) Vascular anomalies: From genetics toward models for therapeutic trials. *Cold Spring Harb Perspect Med* 2(8):a009688.
10. Whitehead KJ, Smith MC, Li DY (2013) Arteriovenous malformations and other vascular malformation syndromes. *Cold Spring Harb Perspect Med* 3(2):a006635.
11. Kawasaki J, et al. (2014) RASA1 functions in EPHB4 signaling pathway to suppress endothelial mTORC1 activity. *J Clin Invest* 124(6):2774–2784.
12. Lawson ND, et al. (2001) Notch signaling is required for arterial-venous differentiation during embryonic vascular development. *Development* 128(19):3675–3683.
13. Kim YH, et al. (2008) Artery and vein size is balanced by Notch and ephrin B2/EphB4 during angiogenesis. *Development* 135(22):3755–3764.
14. Lindskog H, et al. (2014) Molecular identification of venous progenitors in the dorsal aorta reveals an aortic origin for the cardinal vein in mammals. *Development* 141(5): 1120–1128.
15. Carlson TR, et al. (2005) Endothelial expression of constitutively active Notch4 elicits reversible arteriovenous malformations in adult mice. *Proc Natl Acad Sci USA* 102(28): 9884–9889.
16. Murphy PA, et al. (2012) Notch4 normalization reduces blood vessel size in arteriovenous malformations. *Sci Transl Med* 4(117):117ra118.
17. Murphy PA, et al. (2008) Endothelial Notch4 signaling induces hallmarks of brain arteriovenous malformations in mice. *Proc Natl Acad Sci USA* 105(31):10901–10906.
18. Murphy PA, Lu G, Shiah S, Bollen AW, Wang RA (2009) Endothelial Notch signaling is upregulated in human brain arteriovenous malformations and a mouse model of the disease. *Lab Invest* 89(9):971–982.
19. Uyttendaele H, Ho J, Rossant J, Kitajewski J (2001) Vascular patterning defects associated with expression of activated Notch4 in embryonic endothelium. *Proc Natl Acad Sci USA* 98(10):5643–5648.
20. ZhuGe Q, et al. (2009) Notch-1 signalling is activated in brain arteriovenous malformations in humans. *Brain* 132(Pt 12):3231–3241.
21. Miniati D, et al. (2010) Constitutively active endothelial Notch4 causes lung arteriovenous shunts in mice. *Am J Physiol Lung Cell Mol Physiol* 298(2):L169–L177.
22. Kitajewski J (2012) Arteriovenous malformations in five dimensions. *Sci Transl Med* 4(117):117fs113.
23. Kim TN, et al. (2012) Line-scanning particle image velocimetry: An optical approach for quantifying a wide range of blood flow speeds in live animals. *PLoS ONE* 7(6): e38590.
24. Snippert HJ, et al. (2010) Intestinal crypt homeostasis results from neutral competition between symmetrically dividing Lgr5 stem cells. *Cell* 143(1):134–144.
25. Wang L, et al. (2008) Restricted expression of mutant SOD1 in spinal motor neurons and interneurons induces motor neuron pathology. *Neurobiol Dis* 29(3):400–408.
26. Ehling M, Adams S, Benedito R, Adams RH (2013) Notch controls retinal blood vessel maturation and quiescence. *Development* 140(14):3051–3061.
27. Bertozzi CC, Hess PR, Kahn ML (2010) Platelets: Covert regulators of lymphatic development. *Arterioscler Thromb Vasc Biol* 30(12):2368–2371.
28. Thoma R (1893) *Untersuchungen über die Histogenese und Histomechanik des Gefässsytems* (Ferdinand Enke, Stuttgart, Germany). German.
29. Fleischer LH, et al. (1993) Relationship of transcranial Doppler flow velocities and arteriovenous malformation feeding artery pressures. *Stroke* 24(12):1897–1902.
30. Krebs LT, Starling C, Chervonsky AV, Gridley T (2010) Notch1 activation in mice causes arteriovenous malformations phenocopied by ephrinB2 and EphB4 mutants. *Genesis* 48(3):146–150.
31. Larrivée B, et al. (2012) ALK1 signaling inhibits angiogenesis by cooperating with the Notch pathway. *Dev Cell* 22(3):489–500.
32. Pitulescu ME, Schmidt I, Benedito R, Adams RH (2010) Inducible gene targeting in the neonatal vasculature and analysis of retinal angiogenesis in mice. *Nat Protoc* 5(9): 1518–1534.